Transmembrane Protein Structure: Spin Labeling of Bacteriorhodopsin Mutants

CHRISTIAN ALTENBACH, THOMAS MARTI, H. GOBIND KHORANA,* WAYNE L. HUBBELL*

Transmembrane proteins serve important biological functions, yet precise information on their secondary and tertiary structure is very limited. The boundaries and structures of membrane-embedded domains in integral membrane proteins can be determined by a method based on a combination of site-specific mutagenesis and nitroxide spin labeling. The application to one polypeptide segment in bacteriorhodopsin, a transmembrane chromoprotein that functions as a light-driven proton pump is described. Single cysteine residues were introduced at 18 consecutive positions (residues 125 to 142). Each mutant was reacted with a specific spin label and reconstituted into vesicles that were shown to be functional. The relative collision frequency of each spin label with freely diffusing oxygen and membrane-impermeant chromium oxalate was estimated with power saturation EPR (electron paramagnetic resonance) spectroscopy. The results indicate that residues 129 to 131 form a short water-exposed loop, while residues 132 to 142 are membrane-embedded. The oxygen accessibility for positions 131 to 138 varies with a periodicity of 3.6 residues, thereby providing a striking demonstration of an α helix. The orientation of this helical segment with respect to the remainder of the protein was determined.

A LARGE NUMBER OF TRANSMEMBRANE PROTEINS THAT serve various important biological functions, such as receptors, ion channels, cytochrome oxidases, adenosine triphosphatases and transport proteins have been characterized. While DNA sequencing has enabled the derivation of the amino acid sequences of many membrane proteins, structural information on them is limited. Proposals for secondary structure models have been based so far on hydropathy algorithms that approximately deduce membrane-embedded domains (*1*). In particular, independent evidence substantiating, for example, the sizes and boundaries of the individual helical segments that are embedded in the bilayer, and the sizes and structures of the polypeptide regions looped out of the membrane into the aqueous medium is essentially nonexistent.

The available biochemical techniques such as labeling, proteolysis, and immunological methods are inadequate for obtaining precise answers to the above structural problems. Efforts to determine high-resolution structures by crystallographic means are hampered by the lack of a general approach for crystallization. An important exception is the photosynthetic reaction center whose three-dimensional structure has been determined in this way (*2*). Two-dimensional nuclear resonance approaches are limited to proteins of relatively low molecular weight (*3*) and are not applicable to most membrane proteins. Thus, alternative methods of structure determination are desirable, and nitroxide spin labeling in combination with site-specific mutagenesis offers one such approach. We now describe the development and application of spin-labeling technique to the study of bacteriorhodopsin, a seven-helical membrane protein from the purple membrane of the archaebacterium *Halobacterium halobium*.

Bacteriorhodopsin (bR) is a retinal-containing protein that functions as a light-driven proton pump (*4, 5*). Henderson and Unwin have presented a structure determined by electron diffraction from the naturally occurring two-dimensional lattice in the purple membrane (*6*). The electron density maps suggested a structure with seven transmembrane helices, and this feature has been incorporated into most secondary structure models (Fig. 1). Despite the application of techniques such as proteolysis (*7, 8*), immunological probes (*9*), surface labeling (*10*), and neutron diffraction (*11*), the sizes of the helical segments and their orientations have remained uncertain. Thus, a number of models have appeared that show no general agreement regarding these features (*7, 8, 12, 13*).

Considerable insight into the mechanism of light-dependent proton translocation by bR has been obtained. Site-specific mutagenesis in combination with biophysical techniques has aided in the identification of specific residues in the protein that participate in the two major electrogenic steps of the photocycle, namely, the proton release from the protonated Schiff base and the internal reprotonation (*14*). For a full elucidation of the mechanism of proton pumping, a high-resolution structure of bR would be required.

Spin-label relaximetry for protein structure determination. Spin-labeling studies of proteins are generally limited to native sites in the molecule that have specific chemical reactivity, such as the sulfhydryl group of cysteine. Such a severe limitation does not allow arbitrary placement of spin labels. The development of site-directed mutagenesis has made it possible to obtain specific attachment sites for spin labels at any desired position in a protein (*15, 16*). Thus, in colicin E1 the electron paramagnetic resonance (EPR) spectra of a

C. Altenbach and W. L. Hubbell are at the Jules Stein Eye Institute and Department of Chemistry and Biochemistry, University of California Los Angeles, Los Angeles, CA 90024–7008. T. Marti and H. G. Khorana are in the Departments of Biology and Chemistry, Massachusetts Institute of Technology, Cambridge, MA 02139.

*To whom correspondence should be addressed.

sequential series of labeled mutants can reveal secondary structure in the water-soluble protein through a periodic variation in spin-label mobility and solvent exposure (*16*).

We have used a sequential series of spin-labeled bacteriorhodopsin mutants to determine elements of secondary and tertiary structure and to delineate intramembrane domains. However, the analysis was based on a novel determination of the topological distribution of spin-label side chains rather than on the motional state of the spin label. In a sequential series of mutants within a particular transmembrane α helix of a helical bundle protein like bR, there are two obvious topological locations in which a spin label can be positioned: the interior of the protein where it experiences tertiary interactions with side chains of other helices, and the exterior surface where it contacts the hydrocarbon chains of the bilayer. These locations can be distinguished experimentally by measuring the collision frequency between the nitroxide and a freely diffusing paramagnetic probe molecule introduced into the system.

Molecular oxygen (O_2) is an ideal choice for the probe because of its small size and finite solubility in all domains of the system, including the protein interior (*17*). The collision frequency of oxygen with a protein-bound spin label depends on the product of translational diffusion constant and local concentration of oxygen. This product is low in the tightly packed protein interior, and spin labels in this location undergo a low collision frequency. Spin labels facing the hydrocarbon chains of the bilayer undergo high collision frequency, since both diffusion and solubility of oxygen are high in that environment (*18, 19*). In a regular secondary structure like that of a transmembrane α helix in a helical bundle, the topological location, and hence the exposure to oxygen, should vary in a periodic fashion along the sequence. The period is a characteristic of the secondary structure and the phase of the oscillation identifies the faces of highest and lowest oxygen accessibility.

Likewise, it is possible to determine whether a particular residue is exposed to the aqueous medium by measuring the collision frequency of the spin label placed at this site with a water-soluble, paramagnetic probe such as chromium oxalate (CROX) that is restricted to the aqueous phase. Collisions can only occur if the site is located in a water-exposed region of the protein. No collisions with CROX would be observed for a spin label located in the protein or membrane interior.

Relative collision frequencies of the paramagnetic probes O_2 or CROX with the nitroxide spin label are estimated through changes in the nitroxide electron spin-lattice relaxation time, T_1, due to direct collision with the probe. Changes in T_1 can be determined by relaximetric methods such as pulse saturation recovery EPR (*20, 21*) or continuous wave (CW) power saturation EPR (*15, 21, 22*). In the following experiments, the CW saturation method was used. The experimental quantity measured in the saturation experiments is $P_{1/2}$, the power at which the EPR signal amplitude of the central line

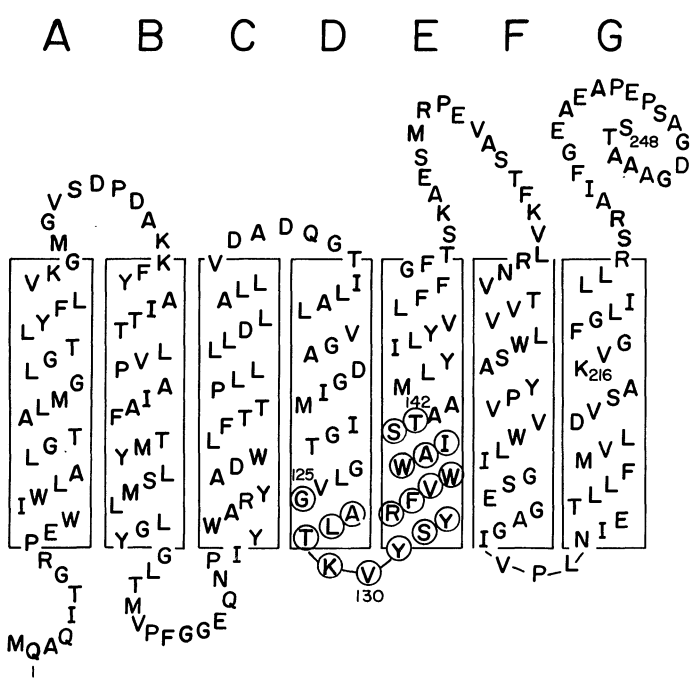

Fig. 1. Location of the mutants in the secondary structure model of bacteriorhodopsin. The boxed regions A to G represent the seven α-helical transmembrane segments. The retinal chromophore is attached as a Schiff base to Lys^{216} in helix G. The residues that were changed to cysteine and modified with a spin label are circled. The model shown is that proposed by Huang *et al.* (*13*). The location and size of the loop connecting helices D and E was rearranged for our data. Abbreviations for the amino acid residues are: A, Ala; C, Cys; D, Asp; E, Glu; F, Phe; G, Gly; H, His; I, Ile; K, Lys; L, Leu; M, Met; N, Asn; P, Pro; Q, Gln; R, Arg; S, Ser; T, Thr; V, Val; W, Trp; and Y, Tyr.

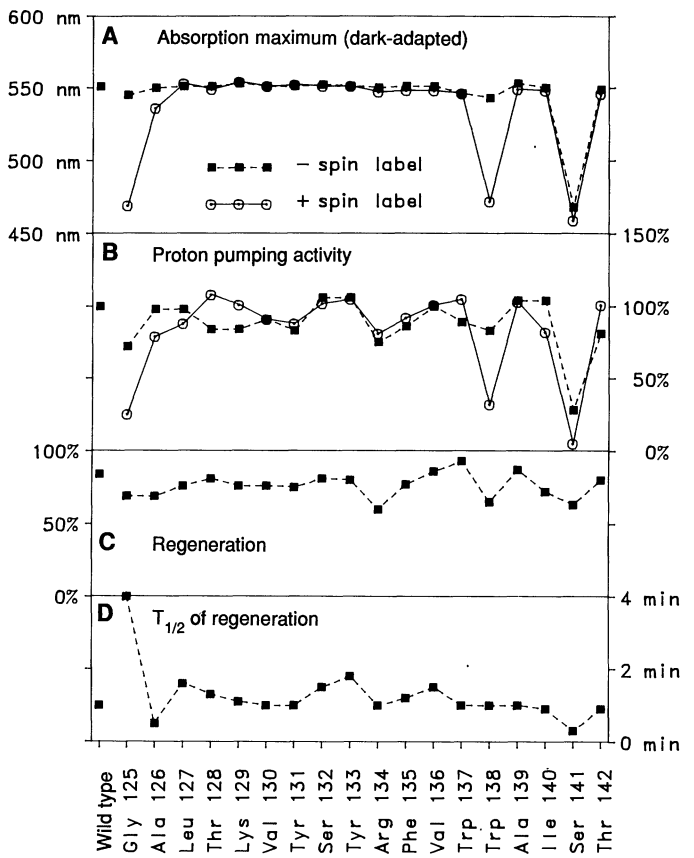

Fig. 2. Spectral and functional characterization of X → Cys mutants and their spin-labeled derivatives. (**A**) Absorption maximum of wild type and the mutants in the dark-adapted form. The spectra of the native proteins (solid squares) were recorded in DMPC-CHAPS micelles (*34*). The spectra of the spin-labeled mutants (open circles) were measured after HPLC gel filtration in OG (*26*). The spectra of the spin-labeled mutants 125 and 138 showed a shoulder at 550 nm. Mutants 125, 138, and 141 were unstable, as indicated by an absorption increase at 380 nm over extended periods of time. Mutant 126 showed a broadened chromophore peak. (**B**) Proton-pumping activity of the mutants as the percentage of wild type (calculated with ϵ = 52,000 M^{-1} cm^{-1}). The native cysteine mutants (solid squares) were measured with the OG dilution method (*34*) (the activity for wild type is 3.2 protons per bR per second). The spin-labeled derivatives (open circles) were measured in the soybean lipid vesicles that were used for the EPR measurements (the activity for wild type is 2.1 protons per bR per second). (**C**) Extent of chromophore regeneration of the native cysteine mutants (calculated with ϵ = 52,000 M^{-1} cm^{-1}). (**D**) Half-time for the rate of chromophore regeneration in minutes (measured at 20°C, with a twofold molar excess of retinal).

is 50 percent of that corresponding to no saturation. The difference between $P_{1/2}$ in the presence and absence of O_2 or CROX is called $\Delta P_{1/2}$ and is proportional to the collision frequency of the nitroxide with the corresponding reagent (*19, 21*).

Bacteriorhodopsin: Functional properties of the cysteine mutants and spin-labeled derivatives. Bacteriorhodopsin is an ideal transmembrane protein with which to explore the application of the method in that much is known about its general structural features. Nevertheless, important structural details remain to be determined. Efficient systems for the expression, purification, and renaturation of bR mutants have been established (*23, 24*). Starting with native bR which contains no cysteine residues, we have introduced single X → Cys substitutions sequentially at positions 125 to 142 (Fig. 1). According to most secondary structure models, this sequence includes portions of the intramembrane helices D and E and the connecting loop (*7, 12, 13*). The mutants were constructed by replacement of the appropriate restriction fragments in the synthetic gene with counterparts containing the altered codons (*24, 25*). After expression in *Escherichia coli*, the mutant proteins were purified to homogeneity as described (*23*). All 18 mutants were then selectively reacted at the single introduced cysteine with a methanethiosulfonate spin label under denaturing conditions (*15*). On subsequent treatment with phospholipids and detergent (*26*), they all folded, bound retinal, and regenerated the bR-like chromophore. Since the regeneration process is not quantitative, the renatured mutants were purified by HPLC gel filtration prior to their reconstitution into soybean phospholipid vesicles (*26*). Bacteriorhodopsin is monomeric at the lipid to protein ratio of 40:1 (w/w) used (*27*).

To monitor the integrity of the structure of the cysteine mutants and their spin-labeled derivatives, we measured kinetics and completeness of regenerations, absorption maxima, and proton-pumping activities (Fig. 2). The absorption maximum (Fig. 2A) is a sensitive indicator for any perturbation of the structure of the retinal binding pocket (*5, 25*). Prior to the attachment of the spin label, only the Ser → Cys mutation of residue 141 induces a sizable shift in the absorption maximum, perhaps because of interaction with the chromophore (*28*). Small but measurable shifts occur also in mutants 125 and 138. After attachment of the spin label, the effect is amplified, these three mutants show large shifts, and mutant 126 becomes slightly shifted. However, a remarkable result is that most spin-labeled mutants are indistinguishable in their absorption spectrum from the wild-type protein.

The proton-pumping activity of the mutants (Fig. 2B) shows almost exactly the same behavior as the absorption maximum. The important conclusion is that all mutants except 125, 138, and 141 show proton-pumping activities comparable to the wild type within the inherent error (±10 percent SD) in the measurement.

The kinetics and efficiencies of regeneration for all mutants are in a relatively narrow range and similar to wild type. The rate of regeneration is slightly slower for the Gly → Cys mutation of residue 125. The very fast regeneration of mutant 141 is perhaps due to an incomplete folding process.

EPR spectra and accessibility to oxygen and CROX. EPR spectra and power saturation data were obtained with the loop gap resonator (LGR) (*15*). The LGR developed by Froncisz and Hyde (*29*) is optimized for limited aqueous samples, and interpretable spectra can be obtained with as little as 10 pmol of labeled protein.

The EPR spectra of all mutants reconstituted in soybean lipid vesicles (Fig. 3) cannot, in general, be simulated with a simple isotropic model of motion and may reflect a distribution of motional states or anisotropic motion (or both). Qualitatively, however, residues 125, 126, 131, 134, 138, 140, and 141 are more motionally restricted relative to the other residues, as judged by the large separation of the outer hyperfine extrema. In contrast, residues 130, 132, 137, and 139 are relatively mobile. As is shown below, these results are consistent with an apparent interior location of the former and surface location of the latter residues. Solubilization of the proteins in 10 percent octyl glucoside (OG) causes a slight increase in mobility of residues 128, 131, 132, 133, and 140, but essentially no change in the others. This indicates that very little structural change occurs upon solubilization in this detergent.

The $\Delta P_{1/2}$ values for O_2 were plotted as a function of sequence position for monomeric bR in phospholipid vesicles (Fig. 4A). In the region of residues 131 to 138, the $\Delta P_{1/2}$, and hence collision frequency with O_2, shows a striking periodicity. A discrete Fourier transform of this limited data set yields a period of 3.60 residues per turn. According to the discussion given above, there is little doubt that this corresponds to an intramembrane α-helical domain of approximately two turns (*30*). The phase of the oscillation fixes the rotational orientation of this helical segment in the protein (Fig. 5); a vector of length proportional to $\Delta P_{1/2}$ points to the corresponding residue from the helix axis. The residues showing the highest collision frequency (largest $\Delta P_{1/2}$) must be facing the lipid bilayer, while those with low $\Delta P_{1/2}$ must be in the protein interior. This then determines the orientation of the helical segment to be that shown in the figure. The resultant of the sum of the individual vectors is another vector that points in the direction of maximum accessibility and serves to determine the segment orientation (dotted vector in Fig. 5). In a theoretical analysis based on the polarity profile and sequence variability of the helices, Rees *et al.* (*31*) predicted the orientations of the helices in bR and defined the direction of residue 134 as most buried inside the protein, in good agreement with our data. When bR mutants were solubilized in 1 percent or 10 percent

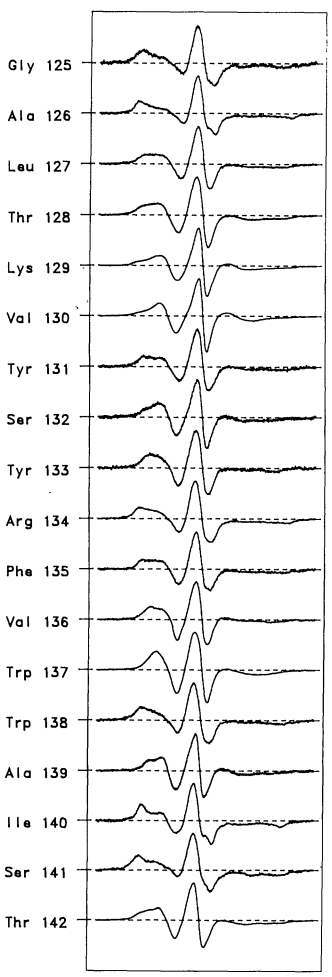

Fig. 3. EPR spectra of spin-labeled bacteriorhodopsin mutants reconstituted in soybean lipid vesicles. Spectra were obtained from samples of bR (2 to 4 μg) in 1 to 2 μl of 50 mM phosphate buffer, pH 6, 150 mM KCl, at room temperature under conditions described previously (*15*). Cysteine residue 141 could not be labeled quantitatively. To obtain an acceptable signal-to-noise ratio, 250 scans were accumulated for this sample.

octyl glucoside (Fig. 4A), essentially identical results were obtained, suggesting that little, if any, conformational change occurs in this region in detergent micelles.

As the spin-label site is moved from residue 139 to 142, a periodicity in $\Delta P_{1/2}$ is still evident, but either the phase or the period begins to change. This may be due to the "tilt" in helix E as inferred from the electron density map (*6*), or an irregularity in the structure imposed by the presence of the retinal chromophore. Indeed, residue 141 is believed to lie within the binding pocket of the β-ionone ring (see below).

The $\Delta P_{1/2}$ values for CROX plotted as a function of sequence position for bR in vesicles, in 1 or 10 percent OG (Fig. 4B) indicates that residues 132 to 142 are inaccessible to collision with CROX; thus, this helical segment is intramembrane. This conclusion is supported by the high value of $\Delta P_{1/2}(O_2)$ for residues exposed on the helical surface (residues 133, 136, and 139). These values are much higher than that for a nitroxide in water, but are consistent with the higher concentration of O_2 in the interior of the bilayer.

As the spin label is moved back in the sequence from residue 131 to 125, the simple periodicity in $\Delta P_{1/2}$ for O_2 is lost. However, another interesting feature emerges and is revealed by the collision frequencies with the water soluble radical CROX. Residues 129 to 131 show a low but measurable accessibility to CROX, indicating exposure to the aqueous phase (Fig. 4B). However, solubilization in 10 percent OG dramatically increases $\Delta P_{1/2}$ for CROX in this region. This effect is not due to unfolding of this region upon solubilization, since the spectral line shapes change relatively little. Rather, the explanation of this effect most likely lies in the high negative charge density of the soybean lipids in which bR is reconstituted (*32*). Since CROX is negatively charged, its surface concentration near the protein is reduced as a result of the negative surface potential. Dissolution in the neutral OG micelles dilutes the negative lipids and diminishes the potential, thus increasing the concentration of CROX near the bR surface. In OG micelles, residues 132 and 133 also seem to become accessible to CROX. This may be due to the dynamic, less structured nature of the micelles relative to the bilayer of the vesicles. The above results support the contention that residues 129, 130, and 131 are exposed to the aqueous phase and represent an interhelical loop region. Several models make definite assignments regarding the loop linking helices D and E. Two models (*12, 13*) postulate a short loop at position 131 to 132, very close to the EPR results, but the loops proposed by Engelman *et al.* (*7*) (residues 128 to 135), and Fimmel *et al.* (*8*) (residues 121 to 133) are significantly larger.

The nitroxides at residues 125 and 126 are highly inaccessible to CROX. They are also inaccessible to O_2, indicating a location within the protein interior. The relatively immobilized line shape for these labels is consistent with this assignment. There is, however, no EPR evidence to indicate whether these residues assume an intramembrane location or are buried inside a structured loop. Residues 127 and 128 show a relatively low collision frequency with O_2. The $\Delta P_{1/2}$(CROX) values in 10 percent OG, where the electrostatic effects are smallest, are comparatively low and so are the values for $\Delta P_{1/2}(O_2)$. This is expected for an interfacial location. As mentioned above, residue 129 is unambiguously exposed to water.

Site-directed spin labeling as a general structural method. Our data show that spin labeling of appropriate X → Cys mutants can yield detailed structural information on bacteriorhodopsin. It is apparent that systematic application of the method should identify all helical domains, their origin and termination sites, and their relative orientations. A major concern in such a study is the possible perturbation of the structure by the spin-label side chain, even though the label is of relatively low molecular volume. In our study, most of the labeled mutants behave similarly to the wild type with regard to functional assays, suggesting a small, if any, perturbation that is due to the nitroxide spin label. The effect of the substitution of Ser^{141} to Cys and its spin-labeled derivative may be due to location of this residue within the binding pocket of the chromophore. This would explain the smaller perturbation imposed by the label at position 138, which is located on the same interior helical surface but one turn away. The lack of a significant effect at position 134 demonstrates that not all labeled residues in the protein interior cause packing problems. Thus, for these three labeled residues the perturbation increases in the order 134, 138, 141, possibly as the binding site of retinal is approached.

The functional assays are expected to be sensitive indicators of perturbation, and function may be lost even with minor structural rearrangement (*33*). Thus, structural inferences based on nitroxide properties may be correct even in unusual cases like 138 and 141, where the presence of the spin label induces large changes in absorption and proton pumping. Evidence for this is seen in the periodic properties of O_2 collision in the region 131 to 138. The

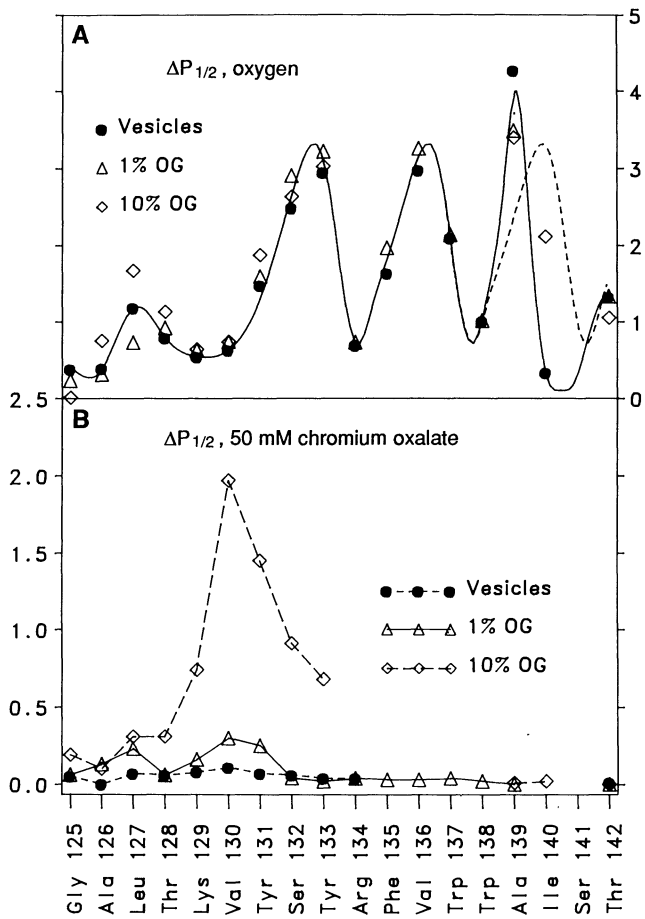

Fig. 4. The accessibility parameter $\Delta P_{1/2}$ for oxygen (**A**) or chromium oxalate (**B**) versus position of the spin label in the bacteriorhodopsin sequence. Power saturation curves were recorded and analyzed as described to obtain $P_{1/2}$ values (*15*). $\Delta P_{1/2}$ values were then obtained by subtraction of the $P_{1/2}$ value in the absence of O_2 or CROX, respectively (this value was always between 0.10 and 0.26). The resonator efficiency was monitored and calibrated by measuring a saturation curve on a solid sample of 1.527E18 spins per gram of DPPH (2,2-diphenyl-1-picryl hydrazyl) in KCl filled into a quartz capillary tube. $P_{1/2}$(DPPH) was 20 to 24 mW and all $P_{1/2}$ values are expressed in multiples of this value. Closed circles are for bacteriorhodopsin mutants reconstituted in soybean lipid vesicles. Open triangles or diamonds are obtained after addition of 1 or 10 percent octyl glucoside, respectively. The estimated error in $\Delta P_{1/2}$ is ±10 percent SD. The dotted line in (A) represents a regular continuation of the periodicity of residues 131 to 138.

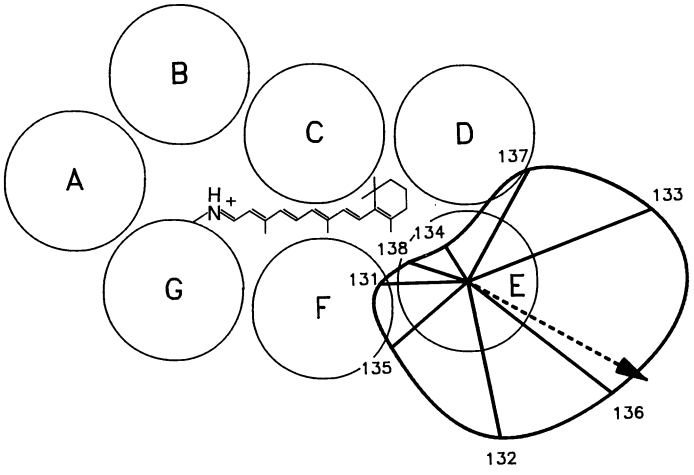

Fig. 5. α-Helical projection of the oxygen accessibility of residues 131 to 138 onto the low-resolution structure of bacteriorhodopsin. The accessibility parameters $\Delta P_{1/2}$ for O_2 are drawn as vectors originating in the axis of helix E. Their length is proportional to $\Delta P_{1/2}$ and the direction increments 100° per residue, characteristic of an α helix. A solid line connects the vector tips and shows the O_2 accessibility profile. This profile was used to deduce the most likely orientation of the helix. The dotted arrow shows the size and direction of the vector sum of the O_2 accessibility.

periodicity is smoothly maintained from residue 131 where there is little perturbation of function to residue 138 where the perturbation is large. Thus properties dependent on structure appear to be invariant in this region while function changes dramatically. The sensitivity to steric perturbation at residue 125 indicates a constrained environment important to protein-chromophore interaction. This notion is consistent with the strongly immobilized line shape of the label at position 125 (Fig. 3).

The classical approach of spin-label line shape analysis is very multidimensional. Line shapes reflect motion, motional anisotropy, environmental polarity, and hydrogen bonding. A line shape generally cannot be reduced to a simple descriptive number reflecting local structure, but only to an array of interacting parameters. However, the O_2 collision frequency and $\Delta P_{1/2}$ give a simple characterization of the topological distribution of the spin-labeled side chains in a sequential series of mutants. This distribution can lead to the identification of regular secondary structure and solvent exposed domains.

In summary, the primary conclusions regarding the structure of bR are: (i) Residues 129 to 131 form a short, water-exposed loop connecting helices D and E. (ii) Residues 132 to 142 are part of transmembrane helix E, with the direction of residue 136 pointing away from the seven helix bundle. (iii) Residues 125 to 128 cannot be unambiguously assigned from the present data, but are likely to be part of transmembrane helix D.

The method described is generally suitable for regular structural determination in membrane proteins. If native cysteines are present, their replacement with a suitable amino acid will maintain the selectivity of the approach (*16*). This strategy allows experimental determination of the water-membrane boundary, identification of water-exposed loop regions, identification of α-helical segments, and determination of the orientation of the helical segments. The method can also identify other secondary and tertiary structures. For example, a β sheet exposed to lipid chains would show an O_2 exposure alternating with every residue and an amphipathic α helix bound to the lipid-water interface would show a periodicity of 3.6 for both O_2 and CROX, but with phases 180° apart.

REFERENCES AND NOTES

1. J. Kyte and R. F. Doolittle, *J. Mol. Biol.* **157**, 105 (1982); H. R. Guy, *Biophys. J.* **47**, 61 (1985); D. Eisenberg, *Annu. Rev. Biochem.* **53**, 595 (1984).
2. J. Deisenhofer and H. Michel, *Science* **245**, 1463 (1989).
3. K. Wüthrich, *ibid.* **243**, 45 (1989).
4. W. Stoeckenius and R. A. Bogomolni, *Annu. Rev. Biochem.* **51**, 587 (1982).
5. H. G. Khorana, *J. Biol. Chem.* **263**, 7439 (1988).
6. R. Henderson and P. N. T. Unwin, *Nature* **257**, 28 (1975).
7. D. M. Engelman, A. Goldman, T. A. Steitz, *Methods Enzymol.* **88**, 81 (1982).
8. S. Fimmel, T. Choli, N. A. Dencher, G. Büldt, B. Wittmann, *Biochim. Biophys. Acta* **978**, 231 (1989).
9. K. Kimura, T. L. Mason, H. G. Khorana, *J. Biol. Chem.* **257**, 2859 (1982); Y. A. Ovchinnikov, *Trends Biochem. Sci.* **12**, 434 (1987).
10. J. Brunner, A. J. Franzusoff, B. Lüscher, C. Zugliani, G. Semenza, *Biochemistry* **24**, 5422 (1985).
11. J. L. Popot, D. M. Engelman, O. Gurel, G. Zaccai, *J. Mol. Biol.* **210**, 829 (1989).
12. D. M. Engelman, R. Henderson, A. D. McLachlan, B. A. Wallace, *Proc. Natl. Acad. Sci. U.S.A.* **77**, 2023 (1980).
13. K. S. Huang, R. Radhakrishnan, H. Bayley, H. G. Khorana, *J. Biol. Chem.* **257**, 13616 (1982).
14. H. Otto *et al.*, *Proc. Natl. Acad. Sci. U.S.A.* **86**, 9228 (1989); H. Otto *et al.*, *ibid.* **87**, 1018 (1990); M. S. Braiman *et al.*, *Biochemistry* **27**, 8516 (1988).
15. C. Altenbach, S. L. Flitsch, H. G. Khorana, W. L. Hubbell, *Biochemistry* **28**, 7806 (1989).
16. A. P. Todd, J. Cong, F. Levinthal, C. Levinthal, W. L. Hubbell, *Proteins* **6**, 294 (1989).
17. D. B. Calhoun, S. W. Englander, W. W. Wright, J. M. Vanderkooi, *Biochemistry* **27**, 8466 (1988).
18. D. A. Windrem and W. Z. Plachy, *Biochim. Biophys. Acta* **600**, 655 (1980).
19. W. K. Subczynski and J. S. Hyde, *ibid.* **643**, 283 (1981).
20. J. S. Hyde, in *Time Domain Electron Spin Resonance*, L. Kevin and R. M. Schwartz, Eds. (Wiley, New York, 1989), pp. 1–30.
21. C. Altenbach, W. Froncisz, J. S. Hyde, W. L. Hubbell, *Biophys. J.* **56**, 1183 (1989).
22. C. P. Poole, *Electron Spin Resonance* (Wiley, New York, 1983).
23. M. S. Braiman, L. J. Stern, B. H. Chao, H. G. Khorana, *J. Biol. Chem.* **262**, 9271 (1987).
24. N. R. Hackett, L. J. Stern, B. H. Chao, K. A. Kronis, H. G. Khorana, *ibid.*, p. 9277.
25. T. Mogi, T. Marti, H. G. Khorana, *ibid.* **264**, 14197 (1989).
26. S. L. Flitsch and H. G. Khorana, *Biochemistry* **28**, 7800 (1989).
27. T. Gulik, M. Seigneuret, J. L. Rigaud, *J. Biol. Chem.* **262**, 15580 (1987).
28. T. Marti and H. G. Khorana, unpublished observations.
29. W. Froncisz and J. S. Hyde, *J. Magn. Reson.* **47**, 515 (1982).
30. The amplitude of the oscillations seen in Fig. 4A will be affected by differences in the transverse relaxation time, T_2, as well as differences in O_2 collision frequency. However, for the mobility range observed here, the effect of T_2 will be to reduce the amplitude variation due to differences in O_2 collision frequency. Hence the differences in collision frequency are actually greater than implied by the data, and the structural conclusions are strengthened.
31. D. C. Rees, L. DeAntonio, D. Eisenberg, *Science* **245**, 510 (1989).
32. T. Gaillard, in *Form and Function of Phospholipids*, G. B. Ansell, J. N. Hawthorne, R. M. C. Dawson, Eds. (Elsevier, Amsterdam, 1973), pp. 253–288.
33. W. A. Lim and R. T. Sauer, *Nature* **339**, 31 (1989).
34. T. Mogi, L. J. Stern, T. Marti, B. H. Chao, H. G. Khorana, *Proc. Natl. Acad. Sci. U.S.A.* **85**, 4148 (1988).

35. C. Altenbach and T. Marti contributed equally to this work. We thank J. Hyde and W. Froncisz and the National Biomedical ESR Center for providing access to the loop gap resonator technology developed at the center (without this device, this work would not have been possible), A. Dereich for machine work in the production of the resonators, and S. Rösselet for technical assistance. Supported by NIH grants EY05216 (W.L.H.) and GM28289 and AI 11479 (H.G.K.), ONR grant N00014-82-K-0668 (H.G.K.), the Jules Stein Professor endowment (W.L.H.), a grant from Research to Prevent Blindness (W.L.H.), and a fellowship from the Swiss National Science Foundation (T.M.)

31 January 1990; accepted 15 April 1990